POLITECNICO DI TORINO
Repository ISTITUZIONALE

Mapping beam cross-section features to higher-order generalized variables using machine learning

Original
Mapping beam cross-section features to higher-order generalized variables using machine learning / Petrolo, M., Pagani, A., Carrera, E., Candita, G., Iannotti, P.. - In: THIN-WALLED STRUCTURES. - ISSN 0263-8231. - ELETTRONICO. - 218:Part C(2026). [10.1016/j.tws.2025.114108]

Availability:
This version is available at: 11583/3004201 since: 2025-10-18T11:35:37Z

Publisher:
Elsevier

Published
DOI:10.1016/j.tws.2025.114108

Terms of use:

This article is made available under terms and conditions as specified in the corresponding bibliographic description in the repository

Publisher copyright

(Article begins on next page)

08 November 2026

Thin–Walled Structures 218 (2026) 114108

Contents lists available at ScienceDirect

Thin-Walled Structures

journal homepage: www.elsevier.com/locate/tws

Full length article

Mapping beam cross-section features to higher-order generalized variables using machine learning

M. Petrolo [*,1], A. Pagani [2], E. Carrera [2], G. Candita [3], P. Iannotti [4]

MUL² Lab, Department of Mechanical and Aerospace Engineering, Politecnico di Torino, Corso Duca degli Abruzzi 24, 10129 Torino, Italy

ARTICLE INFO

Keywords:
CUF
Structural theories
Beams
Neural networks
FEM

ABSTRACT

This paper presents a Machine Learning approach to mapping beam features to higher-order structural theories. The aim is to provide a numerical tool able to assess the accuracy of a set of generalized displacement variables for a given beam geometry. Furthermore, it can provide the most influential generalized variables for a given problem. The training dataset is built on the Carrera Unified Formulation and is based on a combination of fourth-order polynomial expansions. Convolutional and deep neural networks are used to correlate structural theories, geometries, materials, and accuracy. Dynamics problems are considered, and the accuracy is evaluated using natural frequencies. The trained network receives as inputs the problem features, such as the cross-section geometry and material, and a structural theory and estimates its accuracy. The results show that the proposed approach reliably predicts the accuracy of a structural theory. On the other hand, in evaluating the set of most influential generalized variables, the performance of the networks is poorer but still acceptable. In most cases, the accuracy of the natural frequencies is high if 60% of the total fourth-order terms are included; all terms up to the second-order are mandatory, and some third- and fourth-order terms are very influential.

1. Introduction

In structural mechanics, creating accurate 1D and 2D theories is crucial to lowering the computational complexity of 3D models. However, depending on the problem at hand, the accuracy of these theories can vary significantly; that is, a theory that is effective for one structure may not be as accurate for another. Furthermore, common structural features, e.g., material anisotropy or shear deformability, require theories more advanced than the Euler–Bernoulli Beam Theory (EBBT) [1] and the Timoshenko Beam Theory (TBT) [2,3]. Over the years, improvements to EBBT and TBT have been proposed, such as the inclusion of shear correction factors [4], rotary inertia [5], and warping effects [6].

Higher-order theories have been proposed over the last decades to enhance engineering structural theories [7–12] and applied to several problems such as buckling [13], aeroelasticity [14,15], dynamics [16], thick beams [17], and composite beams [18]. Other well-known approaches include the Generalized Beam Theory (GBT) [19] and Variational Asymptotic Beam Sectional Analysis (VABS) [20]. Recent studies apply higher-order models to the analysis of advanced structural problems. Higher-order shear deformation theories have been employed for the thermal buckling and vibration analysis of functionally graded thin-walled box beams [21] and for the study of vibration and buckling behaviors of porous functionally graded beams on variable elastic foundations [22]. Discontinuous Galerkin formulations have been proposed for developing higher-order accurate beam models [23] and for aeroelastic flutter analysis with variable-order structural modeling capabilities [24].

The present work uses the Carrera Unified Formulation (CUF) [25] to build any order structural theories. CUF adopts a formalism allowing the automatic handling of higher-order generalized variables, governing equations, and Finite Element (FE) matrices. Through the Axiomatic/Asymptotic Method (AAM) [26–28] each variable can be assessed to determine the best theories, i.e., set of degrees of freedom, for a given structural problem. AAM, however, frequently results in costly calculations since it necessitates multiple evaluations to assess

* Corresponding author.
E-mail addresses: marco.petrolo@polito.it (M. Petrolo), alfonso.pagani@polito.it (A. Pagani), erasmo.carrera@polito.it (E. Carrera), giulio.candita@polito.it (G. Candita), pierluigi.iannotti@polito.it (P. Iannotti).
[1] Associate Professor.
[2] Professor.
[3] PhD Student.
[4] PhD.

https://doi.org/10.1016/j.tws.2025.114108
Received 30 June 2025; Received in revised form 21 August 2025; Accepted 13 October 2025
Available online 16 October 2025
0263-8231/© 2025 The Authors. Published by Elsevier Ltd. This is an open access article under the CC BY-NC-ND license (http://creativecommons.org/licenses/by-nc-nd/4.0/).

the effectiveness of every generalized variable. The present paper proposes using Machine Learning (ML) to alleviate such computational burden.

The use of ML in structural mechanics [29–31] and, in particular, of finite element analysis [32,33], is gaining increasing interest, due to the possibility of reducing the analysis time and predictive capabilities. Stress prediction [34], structural health monitoring [35,36], and topology optimization [37] are a few of the many possible applications. Moreover, physics-informed neural networks [38] are being developed to improve accuracy. Additionally, the integration of ML with advanced computational techniques for composite structures has been the subject of recent research studies. For instance, a hybrid ML–optimization approach has been created for the stochastic free vibration analysis of graphene platelet–reinforced functionally graded triply periodic minimal surface microplates [39]. Furthermore, probabilistic ML and multi-fidelity analysis have been used together to enhance the efficiency and reliability of composite manufacturing analysis [40]. These methods demonstrate the importance of data-driven approaches in enhancing the analysis and design of composite materials.

The present paper exploits the joint use of a fully connected Deep Neural Network (DNN) [41,42] and a Convolutional Neural Network (CNN) [43–45] to extract beam cross-sectional features and find the best set of generalized unknown variables able to detect the modal shapes and natural frequencies with the lowest computational cost. In previous works [46–48], the authors used ML to assess the role of higher-order generalized variables. The present work aims to use ML in a broader scenario where the problem features concerning geometry and material properties vary. This paper focuses on dynamic analyses because their advantage over static analyses is that they provide, simultaneously, various structural behaviors, such as bending, torsion, and coupling. In past papers, the authors considered static analysis to develop Best Theory Diagrams (BTD) without the use of ML [49,50].

This manuscript is structured as follows: Section 2 presents CUF; Section 3 presents AAM; Section 4 introduces the adopted ML approach; Section 5 presents the results of the work; Section 6 draws the conclusions.

2. Structural theories and finite elements

Fig. 1 shows the reference system adopted for 1D theories with the cross-section lying on the x-z plane. The displacement field's components are the following:

$$\boldsymbol{u}(x,y,z) = \{u_x, u_y, u_z\}^T \tag{1}$$

In CUF, 1D theories the displacement field and its variation are given by expansion functions F_τ and F_s:

$$\boldsymbol{u}(x,y,z) = F_\tau(x,z)\boldsymbol{u}_\tau(y) \qquad \delta\boldsymbol{u}(x,y,z) = F_s(x,z)\delta\boldsymbol{u}_s(y) \tag{2}$$

$$\tau, s = 1, ..., M$$

The Einstein notation acts on τ and s. M denotes the number of terms of the expansion. u_τ is the vector of the generalized displacement variables. For example, a second-order 1D model is given by the following displacement field:

$$\begin{aligned} u_x &= u_{x1} + xu_{x2} + zu_{x3} + x^2u_{x4} + xzu_{x5} + z^2u_{x6} \\ u_y &= u_{y1} + xu_{y2} + zu_{y3} + x^2u_{y4} + xzu_{y5} + z^2u_{y6} \\ u_z &= u_{z1} + xu_{z2} + zu_{z3} + x^2u_{z4} + xzu_{z5} + z^2u_{z6} \end{aligned} \tag{3}$$

It has eighteen generalized variables or Degrees of Freedom (DOF). The FE formulation can be obtained by introducing the shape functions,

$$\boldsymbol{u}(x,y,z) = N_i F_\tau \boldsymbol{u}_{\tau i} \qquad \delta\boldsymbol{u}(x,y,z) = N_j F_s \delta\boldsymbol{u}_{sj} \tag{4}$$

$$i, j = 1, ..., N_n$$

N_i and N_j are the shape functions, N_n is the number of FE nodes, $u_{\tau i}$ and δu_{sj} are the vectors of nodal unknown variables and variations. For

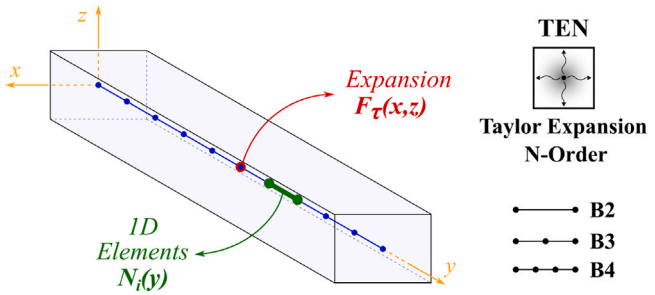

Fig. 1. Reference coordinate system.

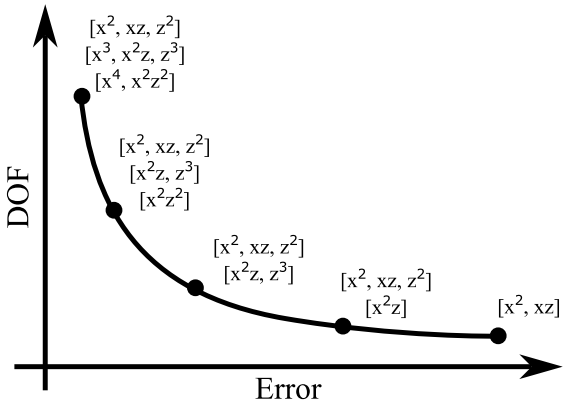

Fig. 2. A Best Theory Diagram (BTD) for 1D theories.

further details on the FE formulation, see [25,51]. The displacement field and the strain components are related through the following geometrical relation:

$$\boldsymbol{\epsilon} = \boldsymbol{b}\boldsymbol{u} \tag{5}$$

Where $\boldsymbol{b}$ is the differential operator matrix [25,51]. In this work, only isotropic linear elastic materials are considered and the Hooke's law is used for the constitutive equation:

$$\boldsymbol{\sigma} = \boldsymbol{C}\boldsymbol{\epsilon} \tag{6}$$

The Principle of Virtual Displacements (PVD) is used to derive the governing differential equations as detailed in [25],

$$\delta L_{int} = \delta L_{ext} - \delta L_{ine} \tag{7}$$

Where L_{int} is the strain energy, L_{ext} is the work of the external forces, and L_{ine} is the work done by the inertial forces. For the free-vibration case, the following governing equations are obtained:

$$\delta\boldsymbol{u}_{sj} : \quad \boldsymbol{m}_{\tau sij}\ddot{\boldsymbol{u}}_{\tau i} + k_{\tau sij}\boldsymbol{u}_{\tau i} = 0 \tag{8}$$

$\mathbf{k}_{\tau sij}$ and $\mathbf{m}_{\tau sij}$ are the fundamental nucleus (FN) of the stiffness matrix and mass matrices, respectively; they are 3×3 matrices independent of the order of the expansion. The global FE matrices - $\mathbf{K}$ and $\mathbf{M}$ - can be obtained by cycling over the four indices - τ, s, i, and j. The natural frequencies ω_n and modal shapes can be obtained by solving the eigenvalue problem,

$$(\boldsymbol{K} - \omega_n^2\boldsymbol{M})\boldsymbol{Q} = 0 \tag{9}$$

3. Axiomatic/asymptotic method

The process of developing structural theories involves choosing the right expansion terms that have the most significant impact on the

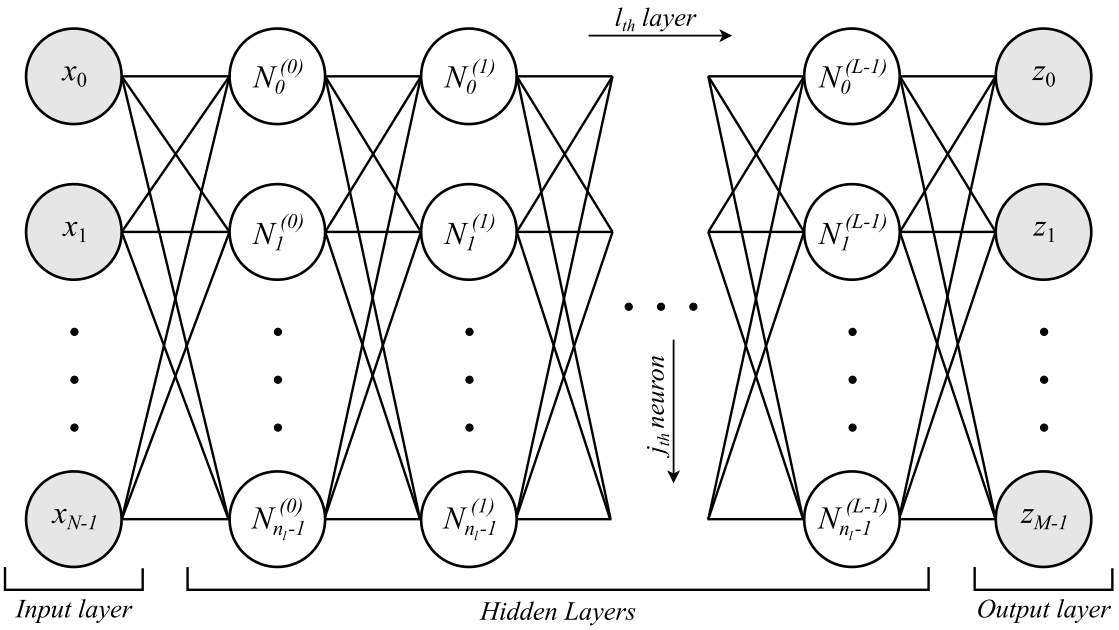

Fig. 3. An example of a deep neural network.

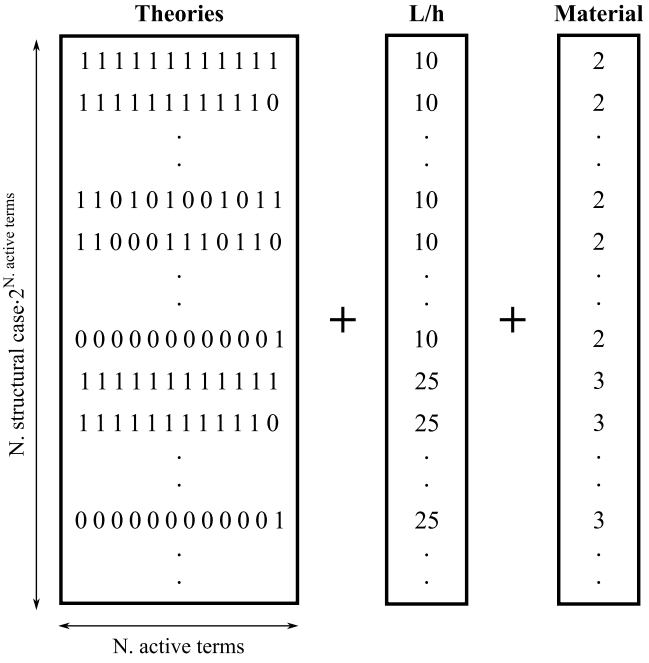

Fig. 4. Input coding for structural theories, L/h ratio, material.

accuracy of the solution. Different sets of generalized unknown variables, or kinematics, can be evaluated and compared using the AAM. A performance parameter such as displacement, stress components, or frequencies determines optimal theories. For a given number of DOF, the AAM outcome is the set of theories resulting in the most accurate numerical results. An example of BTD is shown in Fig. 2, in which each theory is identified by the number of terms, i.e., DOF, and error. This work considered a full fourth-order Taylor expansion 1D theory as the reference solution, N=4, having 15 DOF for each displacement component, i.e.,

$$\begin{aligned} u_x &= u_{x1} + xu_{x2} + zu_{x3} + x^2u_{x4} + xzu_{x5} + \cdots + x^3u_{x7} + \cdots + x^4u_{x11} \\ &\quad + x^3zu_{x12} + \cdots + z^4u_{x15} \\ u_y &= u_{y1} + xu_{y2} + zu_{y3} + x^2u_{y4} + xzu_{y5} + \cdots + x^3u_{y7} + \cdots + x^4u_{y11} \\ &\quad + x^3zu_{y12} + \cdots + z^4u_{y15} \\ u_z &= u_{z1} + xu_{z2} + zu_{z3} + x^2u_{z4} + xzu_{z5} + \cdots + x^3u_{z7} + \cdots + x^4u_{z11} \\ &\quad + x^3zu_{z12} + \cdots + z^4u_{z15} \end{aligned} \tag{10}$$

The accuracy of each theory was evaluated using a percentage relative error $\%E_{AVG}$ over the first ten natural frequencies:

$$\%E_{AVG} = 100 \cdot \frac{1}{n} \sum_{i=1}^{n} \frac{\left| f_i - f_i^{N=4} \right|}{\left| f_i^{N=4} \right|} \tag{11}$$

Where n is the number of modes considered, $f_i^{N=4}$ is the ith frequency of the full fourth-order reference theory, f_i is the ith frequency of the theory to be evaluated, with $i = 1, \ldots, n$. AAM can require a significant amount of numerical analysis as all combinations of expansion terms should be evaluated; e.g., for an N=4 1D theory, which has fifteen generalized unknowns per displacement component, 2^{45} analyses are needed. Furthermore, as the problem inputs change, e.g., boundary conditions or geometry, a new analysis is required. Different strategies can be adopted to lower this number, like excluding specific terms from the procedure by considering them always active. This is typically done for constant and first-order terms, known for their fundamental contribution to obtaining meaningful and accurate results. A second strategy is activating or deactivating all the three expansion terms for all three displacement components, thus leading to 2^{15} required analyses.

4. Neural networks

The present paper aims to use a CNN and a fully connected DNN to obtain the AAM's outcome using just a fraction of the typically required results. Furthermore, problem features are included in the training process to obtain neural networks able to provide the influence of generalized displacements for a given set of material properties and geometry.

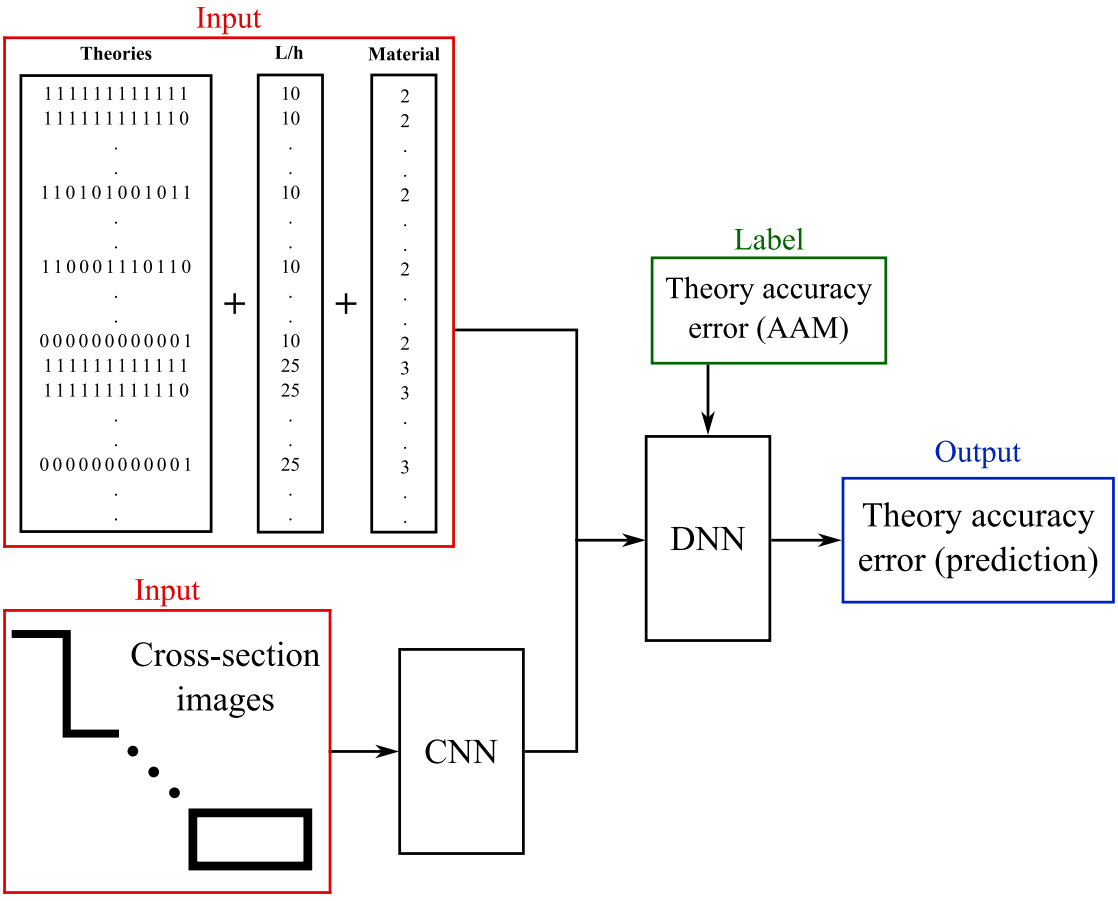

Fig. 5. Global NN architecture.

4.1. Deep and convolutional neural networks

Neural Networks (NN) [52] aim to learn how a system behaves and reproduce that behavior after proper training. Depending on the data type and problem, different learning strategies can be used [53]. This work adopted a supervised learning approach, where the model is trained on labeled data to learn the relationship between inputs and outputs. A typical example is the fully connected DNN, see Fig. 3, which follows the TensorFlow notation. The input vector, **x**, has N elements, the output vector **z** has M elements, and each hidden layer consists of a set of neurons $N_j^{(l)}$. The number of neurons can vary from layer to layer. CNN is an NN typically used for image processing to identify patterns like edges, textures, or more intricate features by using learnable filters to scan small input areas using convolution operations. CNN can be applied to other structured data types, such as time series, text, and other sequential formats, even though they are most commonly utilized in image analysis.

4.2. Coding of structural theories as input of a neural network

A structural theory is an NN input, and generalized displacements are set to 1 or 0; the former indicates an active term, while the latter is deactivated. As an example, an N=2 1D theory can be encoded as follows:

$$\begin{aligned} u_x &= u_{x1} + xu_{x2} + x^2u_{x4} \\ u_y &= u_{y1} + xzu_{y5} \qquad \rightarrow [111\ 100\ 001\ 100\ 010\ 001] \\ u_z &= u_{z1} + zu_{z3} + z^2u_{z6} \end{aligned} \tag{12}$$

Since constant and first-order terms are generally significant to 1D theories, they were always kept active in this paper. This assumption decreases the number of possible structural theory combinations from 2^{45} to 2^{36}. Furthermore, this number decreased to 2^{12} combinations by considering active/inactive all the three expansion terms for a given displacement order, for example,

$$\begin{aligned} u_x &= \cdots + x^2u_{x4} + z^2u_{x6} + x^2zu_{x8} + xz^3u_{x14} + z^4u_{x15} \\ u_y &= \cdots + x^2u_{y4} + z^2u_{y6} + x^2zu_{y8} + xz^3u_{y14} + z^4u_{y15} \rightarrow [1\ 0\ 1\ 0\ 1\ 0\ 0\ 0\ 0\ 0\ 1\ 1] \\ u_z &= \cdots + x^2u_{z4} + z^2u_{z6} + x^2zu_{z8} + xz^3u_{z14} + z^4u_{z15} \end{aligned} \tag{13}$$

The first digit represents the first parabolic term u_{x4}, while the last represents the fourth-order term u_{x15}. It should be noted that, for the two assumptions mentioned before, a 45 DOF theory may be referred to as a 15 DOF one.

4.3. Neural network input

The network architecture adopted in this paper has two inputs. The first is the vector containing the structural theory encoded as in Eq. (13), the slenderness ratio, and the material, as shown in Fig. 4. $N_{\text{structural case}}$ and $N_{\text{active terms}}$ are the number of structural cases and active terms of structural theories considered, respectively. A combination of slenderness ratio and material identifies a structural case. The L/h column contains the real values of the ratio, while in the material column, each value corresponds to a specific material: "2" is aluminum, "3" is titanium, and "4" is steel. It should be noted that, in this work, the "h" parameter in the L/h ratio is the largest side of the cross-section. The second input is the image of the cross-section. The overall architecture of the NN is shown in Fig. 5. Initially, the cross-section images are processed through a CNN. The cross-sections

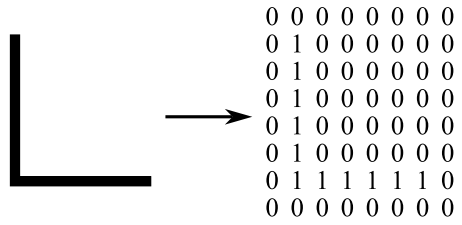

Fig. 6. L-shaped cross-section coding.

Table 1
DNN parameters.

Layer type	Layer size	Activation function
Dense	32	tanh
Dense	32	tanh
Dense	32	tanh
Dense (output)	1	ReLU

are provided as inputs to the CNN in matrix form, coded into 45 × 45 grids; the value "1" is assigned to the cells filled by the cross-section and "0" to the empty cells, see Fig. 6 for an L-shaped cross-section example; for the sake of clarity, a smaller grid was used. The 45x45 grid proved sufficient to define cross-sections with a maximum width of 40 cm and a minimum thickness of 1 cm. Most likely, finer grids will be needed when more complex geometries are considered, e.g., curved cross-sections. The CNN working as a feature extractor in this work is the pre-trained MobileNetV2 [54,55]. The output of this CNN is concatenated to the input in Fig. 4, containing information about the theories, L/h ratio, and materials. As shown in Fig. 5, the concatenated data passes through a DNN, and Table 1 shows the details of the DNN. The network output is the performance parameter from Eq. (11). For the training phase, the output of the DNN is compared with that obtained from AAM analyses.

4.4. Training set size

Each structural case has 2^{12} structural theories, and only a fraction is used to train the DNN. Theories are not evenly distributed by total DOF. For example, there are twelve combinations with fourteen DOF, but 924 combinations with nine DOF. This imbalance may hurt the learning process. To counter this, different inclusion coefficients were applied to avoid medium-DOF cases to dominate the dataset. The number of selected samples for all theories having n DOF is

$$S_n = c_n \times N_n \tag{14}$$

c_n is the inclusion coefficient ranging from 0 to 1, and N_n is the total number of available samples. The S_n theories were randomly selected. S is the total number of training samples for one structural case,

$$S = \sum_n S_n \tag{15}$$

Table 2 reports the distribution of theories for each number of DOF in a single structural case. Three datasets used for network training are presented, each differing in the percentage of included theories with respect to the total computed by AAM. The dataset sizes correspond to 1%, 5%, and 10% of the total number of cases. For instance, in the 10% dataset, S is equal to 427, meaning that 427 training samples were used for each structural case. If there were 100 structural cases, the training dataset would consist of 42700 samples of structural theories.

5. Results

Five cross-sections were used for training the network, as shown in Fig. 7. Tables 3 and 4 show the sets of dimensions and materials

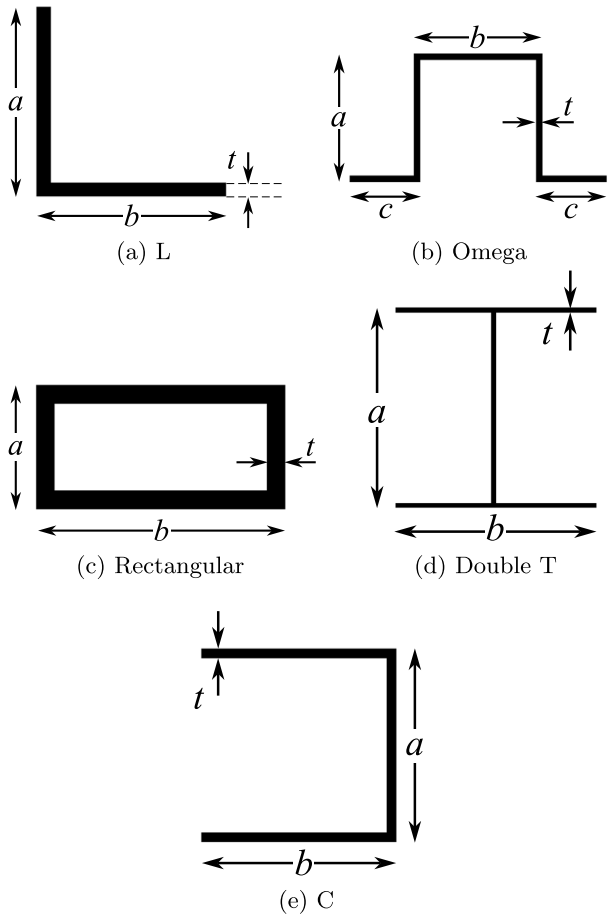

Fig. 7. Cross-sections used for the network training.

adopted for training. For instance, for the C section, nine pairs of a and b, two thicknesses, and three lengths were used. Overall, 738 structural cases were generated. Each case includes 2^{12} structural theory combinations, totaling 3,022,848 FEM modal analyses. A ten B4 structural mesh was used in all cases, and the beam was clamped at one end.

5.1. Selection of the training dataset size

Three sizes of the dataset were tested: 1%, 5%, and 10%. Such percentages refer to the total FEM modal analyses; i.e., the 1% dataset has approximately 39,000 samples. The percentage of theories included in the training dataset is shown in Table 2. The results shown hereafter concern two cross-sections: an Omega and a C. The latter, as shown in Fig. 8, was not included in the training and serves to assess the network's ability to extrapolate results. The geometries and materials are the following:

- Omega: L/h=10, a=20 cm, b=10 cm, c=5 cm, t=1 cm, aluminum
- C: L/h=20, a=40 cm, b=18 cm, c=10 cm, t=2 cm, titanium

h is the largest side of the cross-section; in this case, L/h=L/a. Table 5 shows the first five frequencies for these structural cases computed using N=4.

Fig. 9 shows the BTD of the Omega cross-section. Four diagrams are reported: "AAM" indicates the BTD obtained through FEM modal analysis; for this curve, all the FEM modal analyses for all the structural cases were carried out, which are approximately three million, and only the results relating to the omega section are reported. The other three curves stem from the DNN with different sizes of the training dataset.

Table 2
Percentage of theories included in the training dataset for one structural case and different dataset sizes.

Theory DOF	15	14	13	12	11	10	9	8	7	6	5	4	3
N_n	1	12	66	220	495	792	924	792	495	220	66	12	1
						Dataset 1% - S=53							
	100.0	25.0	4.55	1.82	1.01	0.88	0.87	0.88	1.01	1.82	4.55	25.0	100.0
c_n [%]						Dataset 5% - S=232							
	100.0	25.0	22.7	6.82	5.05	4.73	4.33	4.73	5.05	6.82	22.7	25.0	100.0
						Dataset 10% - S=427							
	100.0	25.0	22.7	13.6	10.1	9.47	8.65	9.47	10.1	13.6	22.7	25.0	100.0

Table 3
Geometries of the cross-sections used for the network training.

Cross-section		Dimensions (cm)	t (cm)	L (m)
C	(a,b)	(10,10)-(10,20)-(10,40)-(20,10)-(20,20)-(20,40)-(40,10)-(40,20)-(40,40)	1–3	2-5-10
T	(a,b)	(10,10)-(10,20)-(10,40)-(20,10)-(20,20)-(20,40)-(40,10)-(40,20)-(40,40)	1–3	2-5-10
L	(a,b)	(10,10)-(20,10)-(20,20)-(40,10)-(40,20)-(40,40)	1–3	2-5-10
Omega	(a,b,c)	(10,10,5)-(10,20,10)-(10,30,5)-(20,10,5)-(20,20,10)-(20,30,5)-(40,10,5)-(40,20,10)-(40,30,5)	1–3	2-5-10
Rectangular	(a,b)	(20,20)-(30,30)-(40,40)-(20,10)-(30,10)-(30,20)-(40,10)-(40,20)	1–3	2-5-10

Table 4
Material properties.

Material	E (GPa)	ν	ρ (g/cm^3)
Aluminium	69	0.33	2.7
Titanium	115	0.30	4.5
Steel	210	0.27	7.8

Table 5
Frequencies of the Omega and C beams.

Cross-section	Frequency (Hz)				
	1st	2nd	3rd	4th	5th
Omega	35.13	50.05	207.8	267.3	289.9
C	2.106	6.824	12.95	16.20	34.82

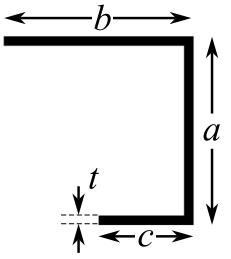

Fig. 8. C cross-section not included in the network training.

This means that only 1%, 5%, and 10% of the three million FEM modal analyses were effectively used to train the DNN. The relative errors between the BTD obtained through the three DNN trained with different training dataset sizes and that derived from AAM computations are available in Fig. 10. Tables 6–9 present the best theories from the four sources. Each row of these tables reports the best theory with a given number of DOF and the error concerning the N=4 structural theory. For instance, the 7-DOF best theory for the Omega cross-section predicted by the AAM has the following terms:

$$\begin{aligned} u_x &= u_{x1} + xu_{x2} + zu_{x3} + xzu_{x5} + z^2u_{x6} + x^3u_{x7} + xz^3u_{x14} \\ u_y &= u_{y1} + xu_{y2} + zu_{y3} + xzu_{y5} + z^2u_{y6} + x^3u_{y7} + xz^3u_{y14} \\ u_z &= u_{z1} + xu_{z2} + zu_{z3} + xzu_{z5} + z^2u_{z6} + x^3u_{z7} + xz^3u_{z14} \end{aligned} \tag{16}$$

Overall, this beam theory has 21 DOF, and the error over the first ten frequencies with respect to the N=4 theory is 4.142%. The results concerning the C cross-section are provided in Figs. 11, 12 and Tables 10–13. The computational times of the simulations run with AAM and DNN are listed in Table 14. It should be noted that AAM only considers the FEM analysis required to build the BTD, encompassing all structural cases and all combinations of structural theories. In contrast, for the DNN approach, the selected dataset comprises 10% of the full AAM dataset. Consequently, nine hours are required for computing the DNN training dataset, in addition to the time spent on DNN training and prediction. These simulations were performed on a computer with the processor "Intel(R) Core(TM) Ultra 7 155H, 1400 Mhz, 16 Core(s), 22 Logical Processor(s)". The results suggest that:

- Overall, the results provided by the NN match well with AAM.
- As expected, the use of larger datasets leads to results closer to AAM concerning the predicted accuracy and the generalized variables composing the best theories.
- More significant differences exist in the results concerning the C cross-section. Such a cross-section was not used during the training set, and the network failed to establish the correct influence of some fourth-order generalized variables. Such DOF are less relevant than the others, and they impact the accuracy by a small amount that may be difficult for the network to detect.

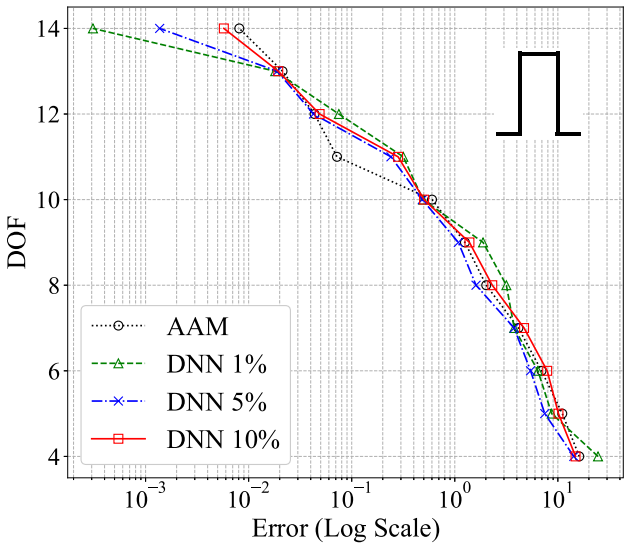

Fig. 9. BTD of the Omega cross-section beam from AAM and neural networks with different training dataset sizes.

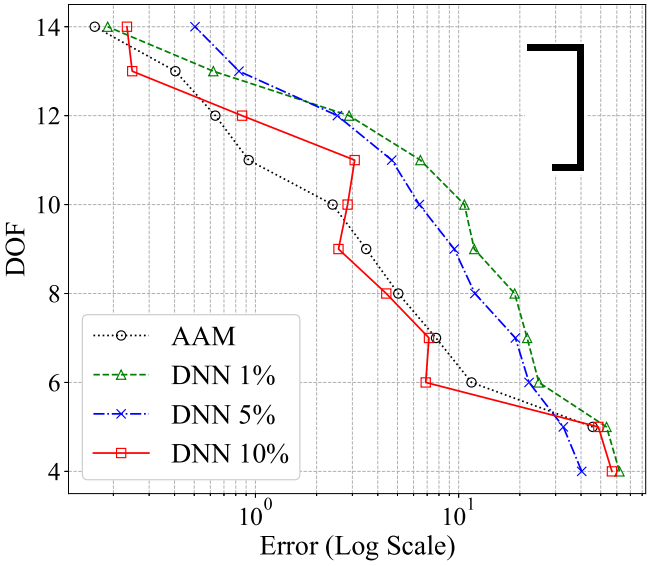

Fig. 11. BTD of the C cross-section beam from AAM and neural networks with different training dataset sizes.

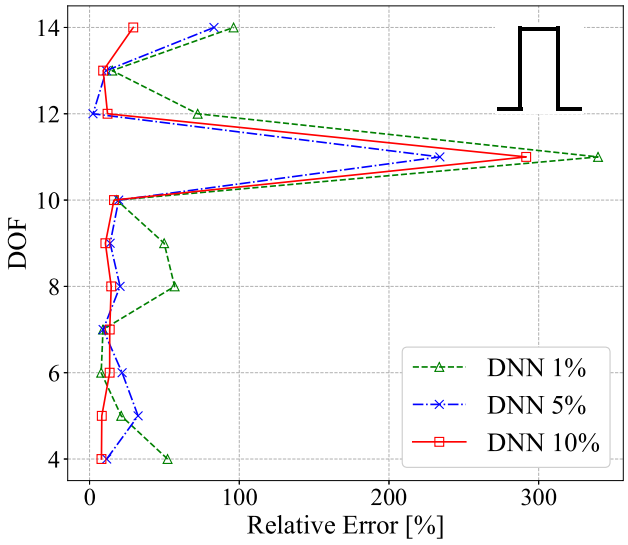

Fig. 10. Error of the BTD from the DNN with different training dataset size and that derived from AAM for the Omega cross-section beam.

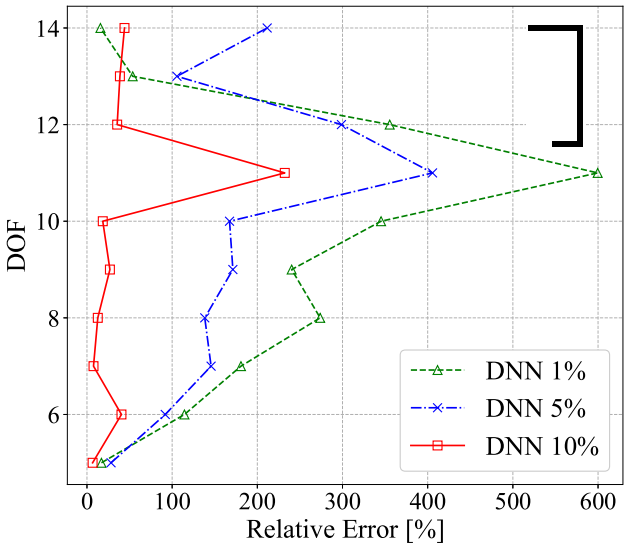

Fig. 12. Error of the BTD from the DNN with different training dataset size and that derived from AAM for the C cross-section beam.

- The 10% dataset is overall more robust and is chosen for all subsequent results. The analysis of the error with respect to AAM shows that the 10% dataset significantly decreases it. Peaks are still present for structural theories with eleven DOF, but the absolute values of the errors associated with these theories are very low in all cases. The computational cost of DNN, including the creation of the dataset, is roughly 10% of the AAM.

5.2. Assessment of neural network with beams included in the training

This section aims to verify NN using cases from the training dataset. The results focus on the following cases:

- Rectangular: L/h=12.5, a=10 cm, b=40 cm, t=3 cm, titanium
- Double T: L/h=25, a=10 cm, b=40 cm, t=1 cm, steel

The first five frequencies for these structural cases obtained by the N=4 model are shown in Table 15. Figs. 13 and 14 show the BTD for the two cases obtained using AAM and the neural network. Tables 16 and 17 show the best theories and their accuracy by AAM and the neural network, for the rectangular beam. The same results concerning the double T are in Tables 18 and 19.

The results suggest the following:

- The neural network effectively predicts the BTD and the accuracy of best theories.
- The generalized variables composing the best theories are very similar when AAM and NN results are compared. In other words, NN successfully maps the problem features and the influence of generalized variables on the solution.

Table 6
Best theories from AAM of the Omega cross-section beam.

DOF	*const.*	x	z	x^2	xz	z^2	x^3	x^2z	xz^2	z^3	x^4	x^3z	x^2z^2	xz^3	z^4	$\%E_{AVG}$
14	▲	▲	▲	▲	▲	▲	▲	▲	▲	▲	▲	▲	△	▲	▲	8.111E−03
13	▲	▲	▲	▲	▲	▲	▲	▲	▲	▲	△	▲	△	▲	▲	2.131E−02
12	▲	▲	▲	▲	▲	▲	▲	▲	▲	▲	△	▲	△	▲	△	4.357E−02
11	▲	▲	▲	▲	▲	▲	▲	△	▲	▲	△	▲	△	▲	△	7.197E−02
10	▲	▲	▲	▲	▲	▲	▲	△	△	▲	△	▲	△	▲	△	6.013E−01
9	▲	▲	▲	▲	▲	▲	▲	△	△	△	△	▲	△	▲	△	1.255E+00
8	▲	▲	▲	▲	▲	▲	▲	△	△	△	△	△	△	▲	△	2.018E+00
7	▲	▲	▲	△	▲	▲	▲	△	△	△	△	△	△	▲	△	4.142E+00
6	▲	▲	▲	△	▲	△	▲	△	△	△	△	△	△	▲	△	6.947E+00
5	▲	▲	▲	△	▲	△	△	△	△	△	△	△	△	▲	△	1.104E+01
4	▲	▲	▲	△	▲	△	△	△	△	△	△	△	△	△	△	1.613E+01

Table 7
Best theories from DNN of the Omega cross-section beam with 1% of training data.

DOF	*const.*	x	z	x^2	xz	z^2	x^3	x^2z	xz^2	z^3	x^4	x^3z	x^2z^2	xz^3	z^4	$\%E_{AVG}$
14	▲	▲	▲	▲	▲	▲	▲	▲	▲	▲	▲	▲	△	▲	▲	3.085E−04
13	▲	▲	▲	▲	▲	▲	▲	▲	▲	▲	▲	▲	△	▲	△	1.809E−02
12	▲	▲	▲	▲	▲	▲	▲	▲	▲	▲	△	▲	△	▲	△	7.504E−02
11	▲	▲	▲	▲	▲	▲	▲	▲	△	▲	△	▲	△	▲	△	3.164E−01
10	▲	▲	▲	▲	▲	▲	▲	△	△	▲	△	▲	△	▲	△	4.920E−01
9	▲	▲	▲	▲	▲	▲	△	△	△	▲	△	▲	△	▲	△	1.880E+00
8	▲	▲	▲	△	▲	▲	△	△	△	▲	△	▲	△	▲	△	3.165E+00
7	▲	▲	▲	△	▲	▲	△	△	△	▲	△	△	△	▲	△	3.770E+00
6	▲	▲	▲	△	▲	▲	△	△	△	△	△	△	△	▲	△	6.408E+00
5	▲	▲	▲	△	▲	△	△	△	△	△	△	△	△	▲	△	8.705E+00
4	▲	▲	▲	△	▲	△	△	△	△	△	△	△	△	△	△	2.453E+01

Table 8
Best theories from DNN of the Omega cross-section beam with 5% of training data.

DOF	*const.*	x	z	x^2	xz	z^2	x^3	x^2z	xz^2	z^3	x^4	x^3z	x^2z^2	xz^3	z^4	$\%E_{AVG}$
14	▲	▲	▲	▲	▲	▲	▲	▲	▲	▲	▲	▲	△	▲	▲	1.370E−03
13	▲	▲	▲	▲	▲	▲	▲	▲	▲	▲	△	▲	△	▲	▲	1.893E−02
12	▲	▲	▲	▲	▲	▲	▲	▲	▲	▲	△	▲	△	▲	△	4.259E−02
11	▲	▲	▲	▲	▲	▲	▲	△	▲	▲	△	▲	△	▲	△	2.404E−01
10	▲	▲	▲	▲	▲	▲	▲	△	△	▲	△	▲	△	▲	△	4.843E−01
9	▲	▲	▲	▲	▲	▲	▲	△	△	▲	△	△	△	▲	△	1.082E+00
8	▲	▲	▲	▲	▲	▲	▲	△	△	△	△	△	△	▲	△	1.607E+00
7	▲	▲	▲	▲	▲	▲	△	△	△	△	△	△	△	▲	△	3.767E+00
6	▲	▲	▲	△	▲	△	▲	△	△	△	△	△	△	▲	△	5.436E+00
5	▲	▲	▲	△	▲	△	△	△	△	△	△	△	△	▲	△	7.460E+00
4	▲	▲	▲	△	▲	△	△	△	△	△	△	△	△	△	△	1.429E+01

Table 9
Best theories from DNN of the Omega cross-section beam with 10% of training data.

DOF	*const.*	x	z	x^2	xz	z^2	x^3	x^2z	xz^2	z^3	x^4	x^3z	x^2z^2	xz^3	z^4	$\%E_{AVG}$
14	▲	▲	▲	▲	▲	▲	▲	▲	▲	▲	▲	▲	△	▲	▲	5.744E−03
13	▲	▲	▲	▲	▲	▲	▲	▲	▲	▲	△	▲	△	▲	▲	1.938E−02
12	▲	▲	▲	▲	▲	▲	▲	▲	▲	▲	△	▲	△	▲	△	4.881E−02
11	▲	▲	▲	▲	▲	▲	▲	△	▲	▲	△	▲	△	▲	△	2.819E−01
10	▲	▲	▲	▲	▲	▲	▲	△	△	▲	△	▲	△	▲	△	5.033E−01
9	▲	▲	▲	▲	▲	▲	▲	△	△	▲	△	△	△	▲	△	1.387E+00
8	▲	▲	▲	▲	▲	△	▲	△	△	△	△	△	△	▲	▲	2.310E+00
7	▲	▲	▲	▲	▲	△	▲	△	△	△	△	△	△	▲	△	4.701E+00
6	▲	▲	▲	▲	▲	△	▲	△	△	△	△	△	△	△	△	7.879E+00
5	▲	▲	▲	△	▲	△	△	△	△	△	△	△	△	▲	△	1.014E+01
4	▲	▲	▲	△	▲	△	△	△	△	△	△	△	△	△	△	1.485E+01

- For the rectangular beam, nine terms per displacement component are necessary to keep the error below 1%. Besides linear terms, all parabolic terms, one cubic and two fourth-order, are required.
- For the double T, fewer terms are needed to have errors smaller than 1%, and the distribution of higher-order terms is similar to the rectangular case.

5.3. Assessment of neural network with beams not included in the training

This section aims to assess the neural network when applied to structural cases not included in the training. The results focus on the following cases, see Fig. 15:

- T: L/h=25, a=20 cm, b=20 cm, t=1 cm, steel
- Z: L/h=5, a=20 cm, b=40 cm, t=3 cm, aluminum

Table 10
Best theories from AAM of the C cross-section beam.

DOF	*const.*	x	z	x^2	xz	z^2	x^3	x^2z	xz^2	z^3	x^4	x^3z	x^2z^2	xz^3	z^4	$\%E_{AVG}$
14	▲	▲	▲	▲	▲	▲	▲	▲	▲	▲	▲	▲	▲	▲	△	1.619E−01
13	▲	▲	▲	▲	▲	▲	▲	▲	▲	▲	△	▲	▲	▲	△	4.036E−01
12	▲	▲	▲	▲	▲	▲	▲	△	▲	▲	△	▲	▲	▲	△	6.347E−01
11	▲	▲	▲	▲	▲	▲	△	△	▲	▲	△	▲	▲	▲	△	9.267E−01
10	▲	▲	▲	▲	▲	▲	△	△	▲	▲	△	▲	△	▲	△	2.396E+00
9	▲	▲	▲	▲	▲	▲	△	△	△	▲	△	▲	△	▲	△	3.507E+00
8	▲	▲	▲	▲	▲	△	△	△	△	▲	△	▲	△	▲	△	5.045E+00
7	▲	▲	▲	△	▲	△	△	△	△	▲	△	▲	△	▲	△	7.739E+00
6	▲	▲	▲	△	▲	△	△	△	△	▲	△	△	△	▲	△	1.157E+01
5	▲	▲	▲	△	▲	▲	△	△	△	△	△	△	△	△	△	4.566E+01
4	▲	▲	▲	△	▲	△	△	△	△	△	△	△	△	△	△	5.437E+01

Table 11
Best theories from DNN of the C cross-section beam with 1% of training data.

DOF	*const.*	x	z	x^2	xz	z^2	x^3	x^2z	xz^2	z^3	x^4	x^3z	x^2z^2	xz^3	z^4	$\%E_{AVG}$
14	▲	▲	▲	▲	▲	▲	▲	▲	▲	▲	▲	▲	△	▲	▲	1.875E−01
13	▲	▲	▲	▲	▲	▲	▲	▲	▲	▲	△	▲	△	▲	▲	6.203E−01
12	▲	▲	▲	▲	▲	▲	▲	▲	▲	▲	△	▲	△	▲	△	2.891E+00
11	▲	▲	▲	▲	▲	▲	△	▲	△	▲	△	△	▲	▲	▲	6.483E+00
10	▲	▲	▲	▲	▲	▲	△	▲	△	▲	△	△	△	▲	▲	1.067E+01
9	▲	▲	▲	▲	▲	△	△	▲	△	▲	△	△	△	▲	▲	1.193E+01
8	▲	▲	▲	△	▲	△	△	▲	△	▲	△	△	△	▲	▲	1.886E+01
7	▲	▲	▲	△	▲	△	△	△	△	▲	△	△	△	▲	▲	2.173E+01
6	▲	▲	▲	△	▲	△	△	△	△	▲	△	△	△	▲	△	2.481E+01
5	▲	▲	▲	△	▲	△	△	△	△	△	△	△	△	▲	△	5.341E+01
4	▲	▲	▲	△	△	△	△	▲	△	△	△	△	△	△	△	6.185E+01

Table 12
Best theories from DNN of the C cross-section beam with 5% of training data.

DOF	*const.*	x	z	x^2	xz	z^2	x^3	x^2z	xz^2	z^3	x^4	x^3z	x^2z^2	xz^3	z^4	$\%E_{AVG}$
14	▲	▲	▲	▲	▲	▲	▲	▲	▲	▲	▲	▲	△	▲	▲	5.044E−01
13	▲	▲	▲	▲	▲	▲	▲	▲	▲	▲	△	▲	▲	▲	△	8.300E−01
12	▲	▲	▲	▲	▲	▲	▲	▲	▲	▲	△	▲	△	▲	△	2.531E+00
11	▲	▲	▲	▲	▲	▲	△	▲	▲	▲	△	▲	△	▲	△	4.686E+00
10	▲	▲	▲	▲	▲	▲	△	▲	△	▲	△	▲	△	▲	△	6.407E+00
9	▲	▲	▲	▲	▲	▲	△	▲	△	▲	△	△	△	▲	△	9.514E+00
8	▲	▲	▲	▲	▲	△	△	▲	△	▲	△	△	△	▲	△	1.202E+01
7	▲	▲	▲	▲	▲	△	△	△	△	▲	△	△	△	▲	△	1.902E+01
6	▲	▲	▲	△	▲	△	△	△	△	▲	△	△	△	▲	△	2.220E+01
5	▲	▲	▲	△	▲	▲	△	△	△	△	△	△	△	△	△	3.275E+01
4	▲	▲	▲	△	▲	△	△	△	△	△	△	△	△	△	△	4.032E+01

Table 13
Best theories from DNN of the C cross-section beam with 10% of training data.

DOF	*const.*	x	z	x^2	xz	z^2	x^3	x^2z	xz^2	z^3	x^4	x^3z	x^2z^2	xz^3	z^4	$\%E_{AVG}$
14	▲	▲	▲	▲	▲	▲	▲	▲	▲	▲	▲	▲	△	▲	▲	2.332E−01
13	▲	▲	▲	▲	▲	▲	▲	▲	▲	▲	△	▲	△	▲	▲	2.475E−01
12	▲	▲	▲	▲	▲	▲	▲	▲	▲	▲	△	▲	△	▲	△	8.598E−01
11	▲	▲	▲	▲	▲	▲	▲	▲	△	▲	△	▲	△	▲	△	3.079E+00
10	▲	▲	▲	▲	▲	▲	△	▲	△	▲	△	▲	△	▲	△	2.841E+00
9	▲	▲	▲	▲	▲	△	△	▲	△	▲	△	△	△	▲	▲	2.562E+00
8	▲	▲	▲	▲	▲	△	△	▲	△	▲	△	△	△	▲	△	4.404E+00
7	▲	▲	▲	▲	▲	△	△	△	△	▲	△	△	△	▲	△	7.144E+00
6	▲	▲	▲	△	▲	△	△	△	△	▲	△	△	△	▲	△	6.885E+00
5	▲	▲	▲	△	▲	△	△	△	△	▲	△	△	△	△	△	4.868E+01
4	▲	▲	▲	△	▲	△	△	△	△	△	△	△	△	△	△	5.677E+01

Table 14
Computational time of AAM and DNN with 10% of training data.

Method	Computational time		
	FEM Analysis	Training	Prediction
AAM	∼90 (h)	–	–
DNN	∼9 (h)	∼2 (min)	< 1 (s)

Table 15
Frequencies of the rectangular and double T beams.

Cross-section	Frequency (Hz)				
	1st	2nd	3rd	4th	5th
Rectangular	3.932	13.94	24.54	68.31	78.90
Double T	1.268	3.202	7.906	19.94	21.97

The first five frequencies for these structural cases obtained by the N=4 theory are shown in Table 20. The BTD are shown in Figs. 16 and 17, whereas the best theories are given in Tables 21–24. The results suggest that:

Table 16
Best theories from AAM of the rectangular beam included in the network training.

DOF	*const.*	x	z	x^2	xz	z^2	x^3	x^2z	xz^2	z^3	x^4	x^3z	x^2z^2	xz^3	z^4	$\%E_{AVG}$
14	▲	▲	▲	▲	▲	▲	▲	▲	▲	▲	▲	▲	△	▲	▲	5.114E−04
13	▲	▲	▲	▲	▲	▲	▲	▲	▲	▲	▲	▲	△	▲	△	5.673E−03
12	▲	▲	▲	▲	▲	▲	▲	▲	▲	▲	△	▲	△	▲	△	1.802E−02
11	▲	▲	▲	▲	▲	▲	▲	▲	△	▲	△	▲	△	▲	△	3.746E−02
10	▲	▲	▲	▲	▲	▲	▲	△	△	▲	△	▲	△	▲	△	2.388E−01
9	▲	▲	▲	▲	▲	▲	△	△	△	▲	△	▲	△	▲	△	6.149E−01
8	▲	▲	▲	▲	▲	▲	△	△	△	▲	△	△	△	▲	△	1.146E+00
7	▲	▲	▲	▲	▲	▲	△	△	△	△	△	△	△	▲	△	2.027E+00
6	▲	▲	▲	▲	▲	▲	△	△	△	△	△	△	△	△	△	3.203E+00
5	▲	▲	▲	▲	▲	△	△	△	△	△	△	△	△	△	△	5.273E+00
4	▲	▲	▲	△	▲	△	△	△	△	△	△	△	△	△	△	8.684E+00

Table 17
Best theories from DNN of the rectangular beam included in the network training.

DOF	*const.*	x	z	x^2	xz	z^2	x^3	x^2z	xz^2	z^3	x^4	x^3z	x^2z^2	xz^3	z^4	$\%E_{AVG}$
14	▲	▲	▲	▲	▲	▲	▲	▲	▲	▲	▲	▲	△	▲	▲	9.128E−03
13	▲	▲	▲	▲	▲	▲	▲	▲	▲	▲	▲	▲	△	▲	△	1.991E−02
12	▲	▲	▲	▲	▲	▲	▲	▲	▲	▲	△	▲	△	▲	△	3.010E−02
11	▲	▲	▲	▲	▲	▲	▲	△	▲	▲	△	▲	△	▲	△	1.770E−01
10	▲	▲	▲	▲	▲	▲	▲	△	△	▲	△	▲	△	▲	△	3.781E−01
9	▲	▲	▲	▲	▲	▲	△	△	△	▲	△	▲	△	▲	△	8.381E−01
8	▲	▲	▲	▲	▲	▲	△	△	△	▲	△	△	△	▲	△	1.278E+00
7	▲	▲	▲	▲	▲	▲	△	△	△	▲	△	△	△	△	△	3.078E+00
6	▲	▲	▲	▲	▲	▲	△	△	△	△	△	△	△	△	△	4.071E+00
5	▲	▲	▲	△	▲	▲	△	△	△	△	△	△	△	△	△	6.519E+00
4	▲	▲	▲	△	▲	△	△	△	△	△	△	△	△	△	△	1.056E+01

Table 18
Best theories from AAM of the double T beam included in the network training.

DOF	*const.*	x	z	x^2	xz	z^2	x^3	x^2z	xz^2	z^3	x^4	x^3z	x^2z^2	xz^3	z^4	$\%E_{AVG}$
14	▲	▲	▲	▲	▲	▲	▲	▲	▲	▲	▲	▲	△	▲	▲	9.177E−05
13	▲	▲	▲	▲	▲	▲	▲	▲	▲	▲	▲	▲	△	▲	△	2.927E−04
12	▲	▲	▲	▲	▲	▲	▲	▲	▲	▲	△	▲	△	▲	△	6.623E−04
11	▲	▲	▲	▲	▲	▲	▲	▲	△	▲	△	▲	△	▲	△	6.926E−03
10	▲	▲	▲	▲	▲	▲	△	▲	△	▲	△	▲	△	▲	△	2.687E−02
9	▲	▲	▲	▲	▲	▲	△	△	△	▲	△	▲	△	▲	△	6.058E−02
8	▲	▲	▲	▲	▲	▲	△	△	△	▲	△	△	△	▲	△	3.223E−01
7	▲	▲	▲	▲	▲	▲	△	△	△	△	△	△	△	▲	△	9.890E−01
6	▲	▲	▲	△	▲	▲	△	△	△	△	△	△	△	▲	△	2.242E+00
5	▲	▲	▲	△	▲	△	△	△	△	△	△	△	△	▲	△	4.330E+00
4	▲	▲	▲	△	△	△	△	△	△	△	△	△	△	▲	△	1.738E+01

Table 19
Best theories from DNN of the double T beam included in the network training.

DOF	*const.*	x	z	x^2	xz	z^2	x^3	x^2z	xz^2	z^3	x^4	x^3z	x^2z^2	xz^3	z^4	$\%E_{AVG}$
14	▲	▲	▲	▲	▲	▲	▲	▲	▲	▲	▲	▲	△	▲	▲	8.426E−04
13	▲	▲	▲	▲	▲	▲	▲	▲	▲	▲	▲	▲	△	▲	△	1.457E−03
12	▲	▲	▲	▲	▲	▲	▲	▲	▲	▲	△	▲	△	▲	△	2.708E−03
11	▲	▲	▲	▲	▲	▲	▲	▲	△	▲	△	▲	△	▲	△	2.057E−02
10	▲	▲	▲	▲	▲	▲	▲	△	△	▲	△	▲	△	▲	△	8.731E−02
9	▲	▲	▲	▲	▲	▲	△	△	△	▲	△	▲	△	▲	△	1.236E−01
8	▲	▲	▲	▲	▲	▲	△	△	△	▲	△	△	△	▲	△	5.184E−01
7	▲	▲	▲	▲	▲	▲	△	△	△	△	△	△	△	▲	△	1.478E+00
6	▲	▲	▲	▲	▲	△	△	△	△	△	△	△	△	▲	△	3.319E+00
5	▲	▲	▲	△	▲	△	△	△	△	△	△	△	△	▲	△	5.904E+00
4	▲	▲	▲	△	▲	△	△	△	△	△	△	△	△	△	△	1.987E+01

- NN can predict the BTD for structural cases not included in the training. However, the predicted error is less accurate than for the beam cases included in the network training but still acceptable.
- The mapping of structural cases to generalized variable influence is less accurate as well; however, it succeeds in highlighting the importance of variables of the same order. The influence of second-order terms is very well detected when compared to third- and fourth-order ones.
- The results strongly depend on the type of section. For instance, at least nine terms per displacement component are necessary to keep the error below 1% in the C-section. In the Z-section case, it is different. Here, for AAM, only 11 terms are required to keep the error below 1%, while DNN is more conservative, showing that fourteen displacement components are necessary.

5.4. Dynamic response of best theories

Best theories were built by using natural frequencies to evaluate their accuracy. This section aims to verify the accuracy of such theories considering modal shapes. The time response is considered, and modal superposition is used to obtain it. The structural cases considered are

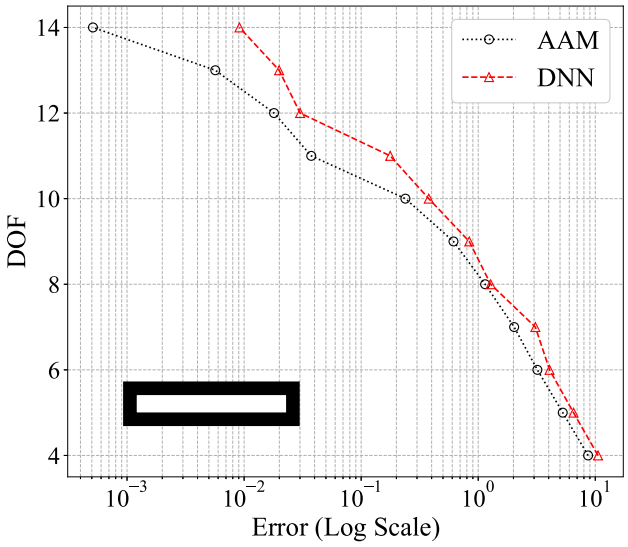

Fig. 13. BTD of the rectangular beam included in the network training.

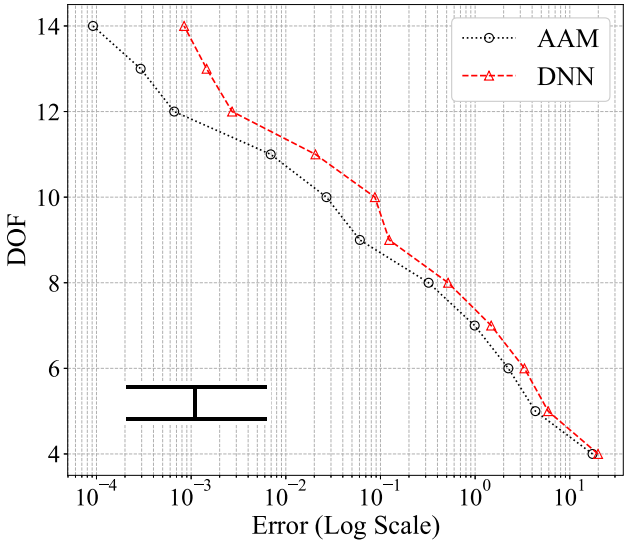

Fig. 14. BTD of the double T beam included in the network training.

Table 20
Frequencies of the T and Z cross-section beams.

Cross-section	Frequency (Hz)				
	1st	2nd	3rd	4th	5th
T	4.803	7.320	28.61	33.86	45.20
Z	33.65	93.00	107.7	200.8	367.1

the Z and C cross-sections analyzed in the previous sections. In the first case, the applied load is sinusoidal, with an amplitude of 1 kN and a frequency of 30 Hz. A step load of the same amplitude is used in the second case. The loading points are shown in Fig. 18, and displacements were evaluated at the same point.

Figs. 19 and 20 show the vertical displacement u_z obtained using modal shapes from best theories with different DOF. The reference is the complete N=4 theory, i.e., fifteen terms per displacement component, while the others have twelve, eight, and four terms per displacement component. Table 25 reports the difference between the reference theory and the lower DOF theories for each structural case. The difference was measured at the sixth positive peak of the reference solution.

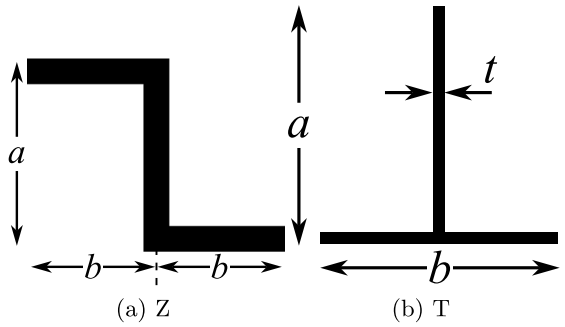

Fig. 15. Z and T cross-sections.

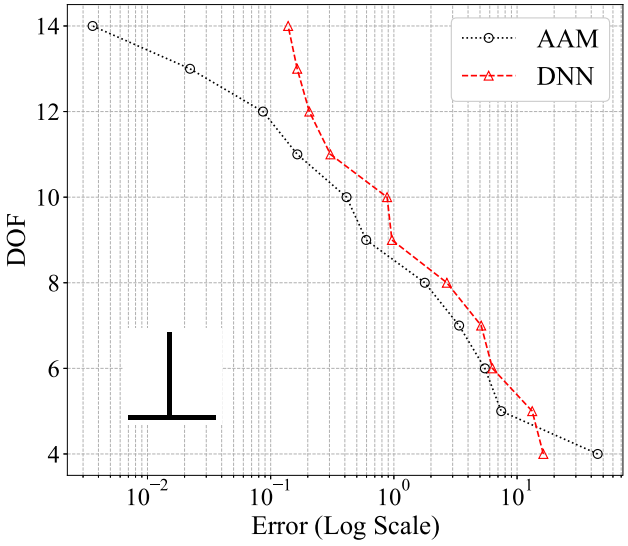

Fig. 16. BTD of the T cross-section beam not included in the network training.

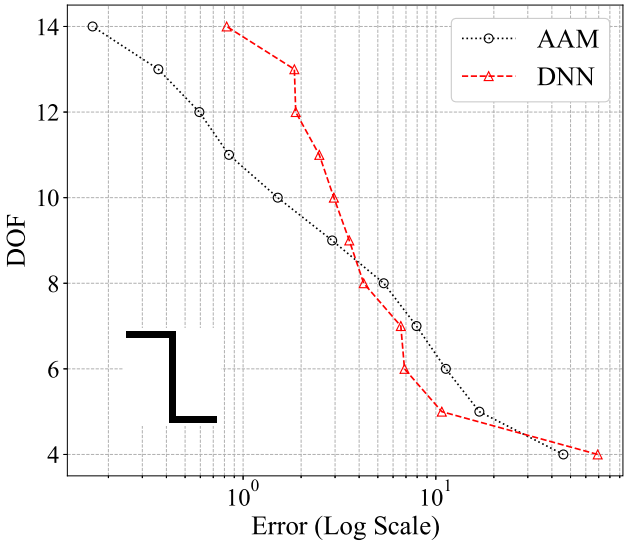

Fig. 17. BTD of the Z cross-section beam not included in the network training.

Table 21
Best theories from AAM of the T cross-section beam not included in the network training.

DOF	*const.*	x	z	x^2	xz	z^2	x^3	x^2z	xz^2	z^3	x^4	x^3z	x^2z^2	xz^3	z^4	$\%E_{AVG}$
14	▲	▲	▲	▲	▲	▲	▲	△	▲	▲	▲	▲	▲	▲	▲	3.586E−03
13	▲	▲	▲	▲	▲	▲	▲	△	▲	▲	△	▲	▲	▲	▲	2.214E−02
12	▲	▲	▲	▲	▲	▲	▲	△	▲	▲	△	▲	△	▲	▲	8.657E−02
11	▲	▲	▲	▲	▲	▲	▲	△	▲	▲	△	▲	△	▲	△	1.645E−01
10	▲	▲	▲	▲	▲	▲	▲	△	△	△	△	▲	△	▲	▲	4.129E−01
9	▲	▲	▲	▲	▲	▲	▲	△	△	△	△	▲	△	▲	△	5.960E−01
8	▲	▲	▲	△	▲	△	▲	△	△	△	△	▲	▲	▲	△	1.783E+00
7	▲	▲	▲	△	▲	△	▲	△	△	△	△	▲	△	▲	△	3.386E+00
6	▲	▲	▲	△	▲	△	▲	△	△	△	△	△	△	▲	△	5.479E+00
5	▲	▲	▲	△	▲	△	△	△	△	△	△	△	△	▲	△	7.438E+00
4	▲	▲	▲	△	▲	△	△	△	△	△	△	△	△	△	△	4.512E+01

Table 22
Best theories from DNN of the T cross-section not included in the network training.

DOF	*const.*	x	z	x^2	xz	z^2	x^3	x^2z	xz^2	z^3	x^4	x^3z	x^2z^2	xz^3	z^4	$\%E_{AVG}$
14	▲	▲	▲	▲	▲	▲	▲	▲	▲	▲	▲	▲	△	▲	▲	1.386E−01
13	▲	▲	▲	▲	▲	▲	▲	▲	▲	▲	△	▲	△	▲	▲	1.641E−01
12	▲	▲	▲	▲	▲	▲	▲	▲	▲	▲	△	▲	△	▲	△	2.059E−01
11	▲	▲	▲	▲	▲	▲	▲	△	▲	▲	△	▲	△	▲	△	3.056E−01
10	▲	▲	▲	▲	▲	▲	▲	△	▲	△	△	▲	△	▲	△	8.812E−01
9	▲	▲	▲	▲	▲	▲	▲	△	△	△	△	▲	△	▲	△	9.643E−01
8	▲	▲	▲	▲	▲	▲	▲	△	△	△	△	▲	△	△	△	2.693E+00
7	▲	▲	▲	▲	▲	△	▲	△	△	△	△	△	△	▲	△	5.113E+00
6	▲	▲	▲	▲	▲	△	▲	△	△	△	△	△	△	△	△	6.314E+00
5	▲	▲	▲	△	▲	△	▲	△	△	△	△	△	△	△	△	1.327E+01
4	▲	▲	▲	△	▲	△	△	△	△	△	△	△	△	△	△	1.634E+01

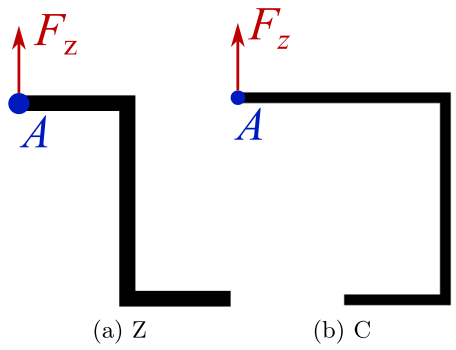

Fig. 18. Loading points for dynamic response analysis.

Table 23
Best theories from AAM of the Z cross-section beam not included in the network training.

DOF	*const.*	x	z	x^2	xz	z^2	x^3	x^2z	xz^2	z^3	x^4	x^3z	x^2z^2	xz^3	z^4	$\%E_{AVG}$
14	▲	▲	▲	▲	▲	▲	▲	▲	△	▲	▲	▲	▲	▲	▲	1.656E−01
13	▲	▲	▲	▲	▲	▲	▲	▲	△	▲	▲	▲	▲	▲	△	3.633E−01
12	▲	▲	▲	▲	▲	▲	▲	▲	△	▲	△	△	▲	▲	▲	5.929E−01
11	▲	▲	▲	▲	▲	▲	▲	▲	△	▲	△	△	▲	▲	△	8.451E−01
10	▲	▲	▲	▲	▲	▲	△	△	▲	▲	△	△	▲	▲	△	1.513E+00
9	▲	▲	▲	▲	▲	▲	△	△	▲	△	△	△	▲	▲	△	2.899E+00
8	▲	▲	▲	▲	▲	▲	△	△	▲	△	△	△	△	▲	△	5.365E+00
7	▲	▲	▲	▲	▲	△	△	△	▲	△	△	△	△	▲	△	7.939E+00
6	▲	▲	▲	▲	▲	△	△	△	△	△	△	△	△	▲	△	1.127E+01
5	▲	▲	▲	△	▲	△	△	△	△	△	△	△	△	▲	△	1.682E+01
4	▲	▲	▲	▲	△	△	△	△	△	△	△	△	△	△	△	4.590E+01

As expected, increasing the DOF of the theory leads to a convergence of the solution towards the reference theory. Depending on the case, eight or twelve terms are necessary to have negligible errors. Further verifications were carried out by using the Modal Assurance Criterion (MAC) [56,57]. Figs. 21 and 22 display the MAC matrices for the Z and C beams, comparing the reference solution with the best theories that include twelve, eight, and four terms. Higher differences in the dynamic responses are clearly associated to off-diagonal terms in the MAC matrix.

6. Conclusions

This paper proposes a methodology for mapping beam features to higher-order generalized displacement variables. The aim is to provide a tool able to estimate the accuracy of a beam theory for a given problem and establish the minimum number of DOF required for reliable results. The proposed methodology uses NN to correlate structural theories, geometries, materials, and accuracy. In particular, CNN and DNN are used. The training dataset is built using the Carrera Unified

Table 24
Best theories from DNN of the Z cross-section beam not included in the network training.

DOF	*const.*	x	z	x^2	xz	z^2	x^3	x^2z	xz^2	z^3	x^4	x^3z	x^2z^2	xz^3	z^4	$\%E_{AVG}$
14	▲	▲	▲	▲	▲	▲	▲	▲	▲	▲	△	▲	▲	▲	▲	8.216E−01
13	▲	▲	▲	▲	▲	▲	▲	▲	▲	▲	△	▲	△	▲	▲	1.845E+00
12	▲	▲	▲	▲	▲	▲	▲	▲	▲	▲	△	▲	△	▲	△	1.875E+00
11	▲	▲	▲	▲	▲	▲	△	▲	△	▲	△	▲	△	▲	▲	2.485E+00
10	▲	▲	▲	▲	▲	△	△	▲	△	▲	△	▲	△	▲	▲	2.958E+00
9	▲	▲	▲	▲	▲	▲	△	△	△	▲	△	▲	△	▲	△	3.556E+00
8	▲	▲	▲	▲	▲	▲	△	△	△	△	△	▲	△	▲	△	4.224E+00
7	▲	▲	▲	▲	▲	▲	△	△	△	△	△	△	△	▲	△	6.582E+00
6	▲	▲	▲	△	▲	▲	△	△	△	△	△	△	△	▲	△	6.879E+00
5	▲	▲	▲	△	▲	△	△	△	△	△	△	△	△	▲	△	1.074E+01
4	▲	▲	▲	△	▲	△	△	△	△	△	△	△	△	△	△	6.915E+01

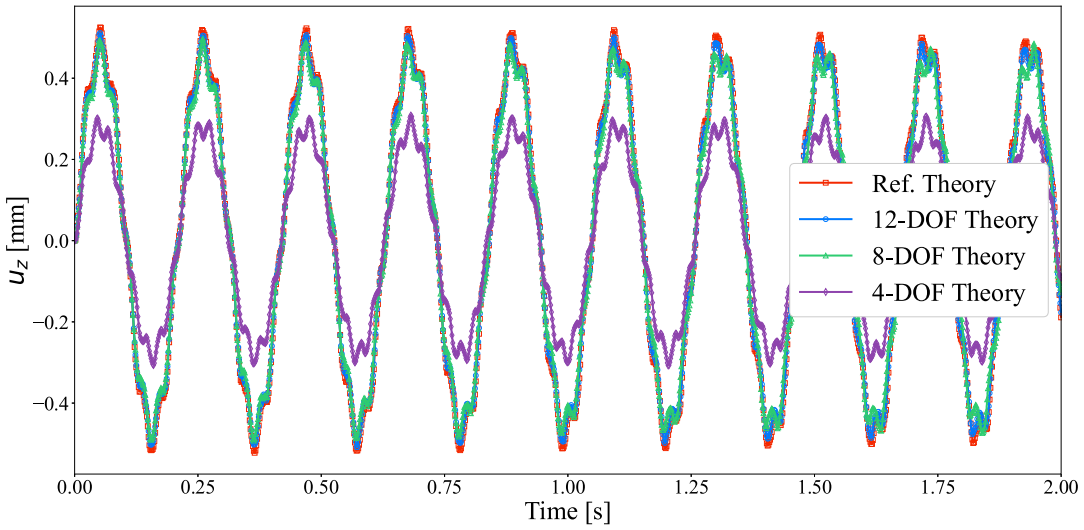

Fig. 19. Time response of the Z cross-section beam from different best theories.

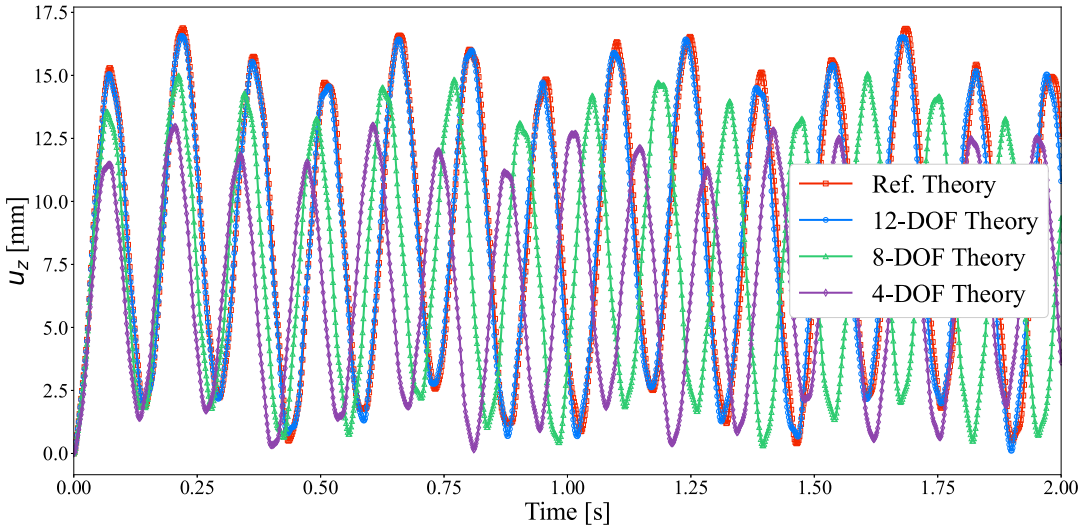

Fig. 20. Time response of the C cross-section beam from different best theories.

Formulation, which can provide FEM solutions for beam theories of any order. Refined beam theories were obtained using a reference fourth-order Taylor expansion and combinations of the terms composing the full expansion. The accuracy was evaluated considering the natural frequencies of the structure, and various cross-section geometries were considered. The results were verified using a comprehensive set of FEM analyses that encompassed all samples derived from the combinations of all cases. At the same time, the network was trained on 10% of the complete dataset. The following conclusions may be drawn:

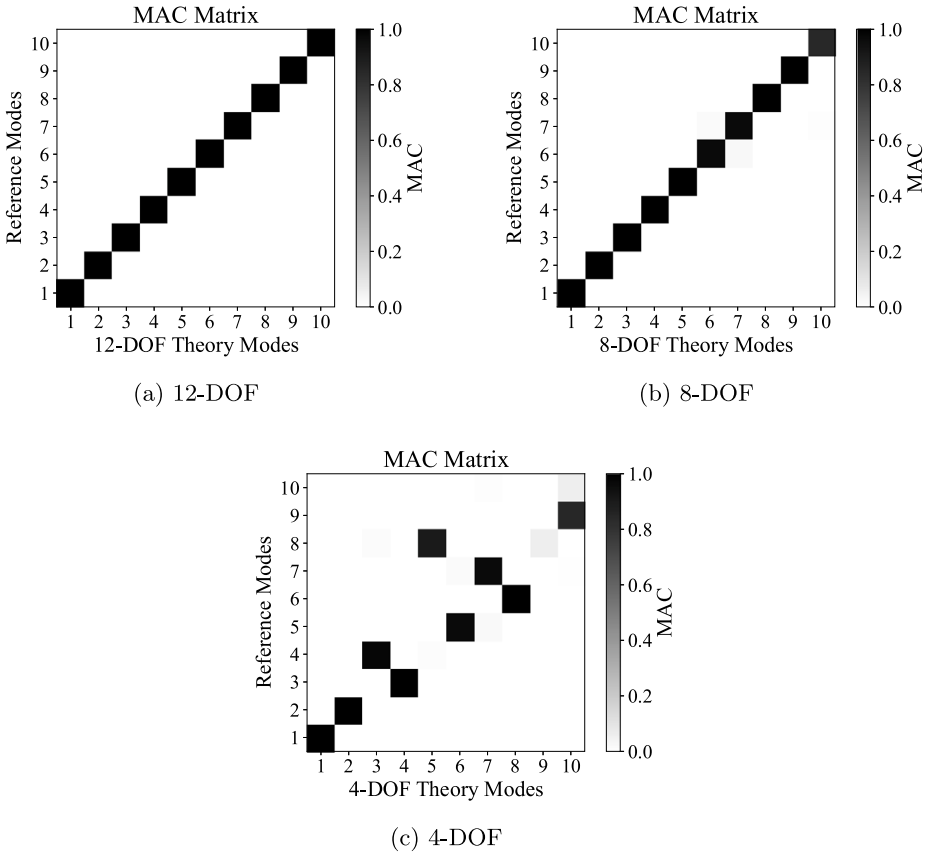

Fig. 21. MAC matrix for the Z cross-section beam.

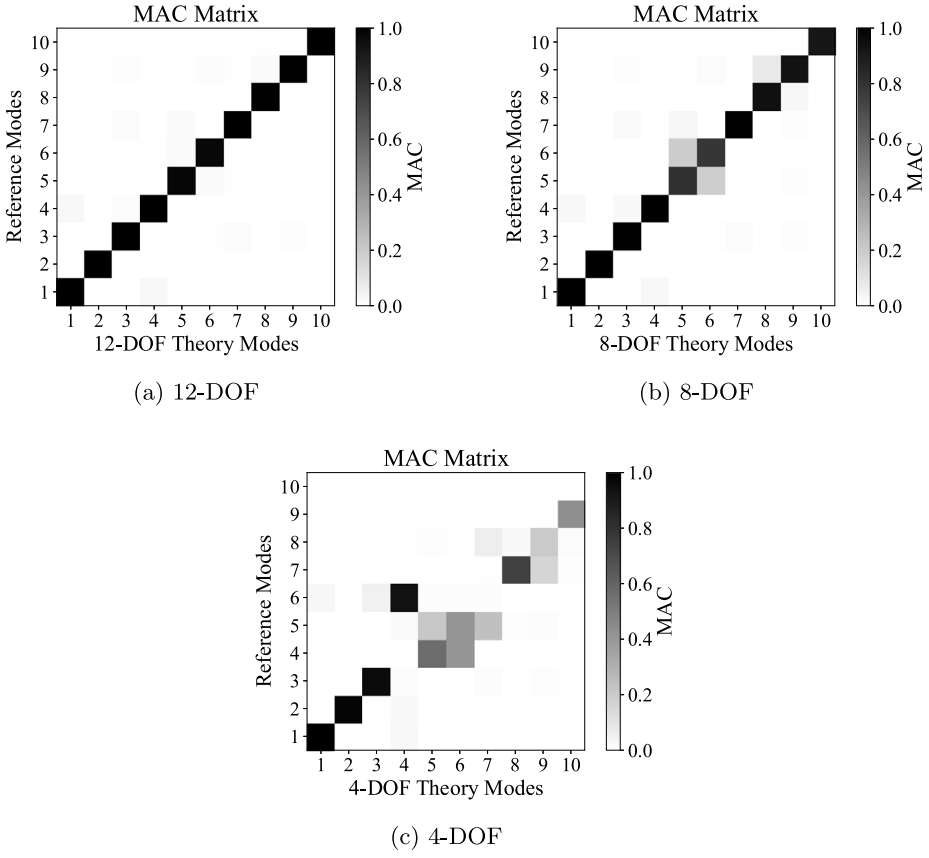

Fig. 22. MAC matrix for the C cross-section beam.

Table 25
Comparison of peak displacements.

Structural case		Theory			
		15-DOF	12-DOF	8-DOF	4-DOF
Z	Time (s)	1.093	1.093	1.092	1.090
	u_z Difference (%)	0.0	3.360	8.780	42.81
		15-DOF	12-DOF	8-DOF	4-DOF
C	Time (s)	1.100	1.095	1.050	1.017
	u_z Difference (%)	0.0	2.570	13.02	22.33

- Overall, the proposed methodology provided satisfactory results when compared to FEM analysis. In fact, with 10% of the computational cost of FEM, there was a good match in terms of accuracy and mapping.
- The accuracy predicted by the network matched very well in all cases. In other words, the network can estimate the accuracy of a set of generalized variables given the geometry of the beam.
- The network performance is less robust in finding the set of most important generalized variables.
- In many cases, at least eight generalized variables per displacement component are required to achieve errors lower than 1%. However, the minimum number of unknowns strongly depends on the type of section and can be higher than ten, e.g., for Z-sections. All terms up to the second order are necessary, and some third- and fourth-order terms must be included. The number of minimum DOF increases if modal shapes are considered.

Future works will explore different NN architectures, including unsupervised learning. Moreover, the optimization of the 3D distribution of theories will be investigated through the node-dependent kinematics approach, allowing to assign to each node a different structural theory and set of DOF. Furthermore, the extension of this work to more complex geometries, curved cross-sections, composites, buckling, and nonlinear analyses will be considered.

CRediT authorship contribution statement

M. Petrolo: Writing – review & editing, Supervision, Methodology, Investigation, Conceptualization. **A. Pagani:** Writing – review & editing, Supervision, Methodology, Investigation, Conceptualization. **E. Carrera:** Writing – review & editing, Methodology, Investigation, Conceptualization. **G. Candita:** Writing – original draft, Visualization, Validation, Methodology, Investigation, Formal analysis, Data curation, Conceptualization. **P. Iannotti:** Writing – review & editing, Supervision, Methodology, Investigation, Data curation, Conceptualization.

Declaration of competing interest

The authors declare that they have no known competing financial interests or personal relationships that could have appeared to influence the work reported in this paper.

Acknowledgments

This publication is part of the project PNRR-NGEU which has received funding from the MUR – DM 117/2023, Italy.

Data availability

Data will be made available on request.

References

[1] L. Euler, De curvis elasticis, 1744, Lausanne Geneva: Bousquet.
[2] S.P. Timoshenko, On the transverse vibrations of bars of uniform cross-section, Lond. Edinb. Dublin Philos. Mag. J. Sci. 43 (253) (1922) 125–131.
[3] S.P. Timoshenko, On the correction for shear of the differential equation fortransverse vibrations of prismatic bars, Lond. Edinb. Dublin Philos. Mag. J. Sci. 41 (245) (1921) 744–746.
[4] F. Gruttmann, W. Wagner, Shear correction factors in timoshenko's beam theory for arbitrary shaped cross-sections, Comput. Mech. 27 (3) (2001) 199–207.
[5] W. Carnegie, J. Thomas, The effects of shear deformation and rotary inertia on the lateral frequencies of cantilever beams in bending, J. Eng. Ind. (1972).
[6] M. Levinson, A new rectangular beam theory, J. Sound Vib. 74 (1) (1981) 81–87.
[7] R.K. Kapania, S. Raciti, Recent advances in analysis of laminated beams and plates. part i-shear effects and buckling, AIAA J. 27 (7) (1989) 923–935.
[8] R.K. Kapania, S. Raciti, Recent advances in analysis of laminated beams and plates, part ii: vibrations and wave propagation, AIAA J. 27 (7) (1989) 935–946.
[9] E. Carrera, M. Petrolo, On the effectiveness of higher-order terms in refined beam theories, J. Appl. Mech. 78 (2) (2010) 021013.
[10] E. Carrera, A. Pagani, M. Petrolo, E. Zappino, Recent developments on refined theories for beams with applications, Mech. Eng. Rev. 2 (2) (2015) 14–00298.
[11] A.S. Sayyad, Y.M. Ghugal, Bending, buckling and free vibration of laminated composite and sandwich beams: A critical review of literature, Compos. Struct. 171 (2017) 486–504.
[12] E. Ruocco, J.N. Reddy, Analytical solutions of Reddy, Timoshenko and Bernoulli beam models: A comparative analysis, Eur. J. Mech. A Solids 99 (2023) 104953.
[13] A.K. Argyridi, E.J. Sapountzakis, Higher order beam theory for linear local buckling analysis, Eng. Struct. 177 (2018) 770–784.
[14] L. Librescu, O. Song, On the static aeroelastic tailoring of composite aircraft swept wings modelled as thin-walled beam structures, Compos. Eng. 2 (5–7) (1992) 497–512.
[15] Z. Qin, L. Librescu, On a shear-deformable theory of anisotropic thin-walled beams: further contribution and validations, Compos. Struct. 56 (4) (2002) 345–358.
[16] D. Shin, S. Choi, G.-W. Jang, Y.Y. Kim, Higher-order beam theory for static and vibration analysis of composite thin-walled box beam, Compos. Struct. 206 (2018) 140–154.
[17] J. Petrolito, Stiffness analysis of beams using a higher-order theory, Comput. Struct. 55 (1) (1995) 33–39.
[18] G. Giunta, F. Biscani, S. Belouettar, A.J.M. Ferreira, E. Carrera, Free vibration analysis of composite beams via refined theories, Compos. Part B: Eng. 44 (1) (2013) 540–552.
[19] C. Mittelstedt, Generalized beam theory for the analysis of thin-walled structures — A state-of-the-art survey, Thin-Walled Struct. 200 (2024) 111849.
[20] W. Yu, D.H. Hodges, J.C. Ho, Variational asymptotic beam sectional analysis – an updated version, Internat. J. Engrg. Sci. 59 (2012) 40–64, The Special Issue in honor of VICTOR L. BERDICHEVSKY.
[21] T.-N. Nguyen, T.-K. Nguyen, X.-B. Bui, T.P. Vo, Thermal buckling and vibration analysis of functionally graded thin-walled box beams using a higher-order shear deformation theory, Mech. Based Des. Struct. Mach. (2025) 1–24.
[22] F. Mellal, R. Bennai, M. Avcar, M. Nebab, H.A. Atmane, On the vibration and buckling behaviors of porous FG beams resting on variable elastic foundation utilizing higher-order shear deformation theory, Acta Mech. 234 (9) (2023) 3955–3977.
[23] V. Gulizzi, I. Benedetti, A. Milazzo, High-order accurate beam models based on discontinuous Galerkin methods, Aerotec. Missili Spaz. 102 (4) (2023) 293–308.
[24] F. Montano, D. Campagna, I. Dimino, V. Gulizzi, I. Benedetti, A discontinuous Galerkin framework for aeroelastic flutter analysis with variable-order structural modeling capability, Mech. Adv. Mater. Struct. (2025) 1–18.
[25] E. Carrera, M. Cinefra, M. Petrolo, Zappino E., Finite Element Analysis of Structures Through Unified Formulation, John Wiley & Sons, 2014.
[26] M. Petrolo, E. Carrera, Best theory diagrams for multilayered structures via shell finite elements, Adv. Model. Simul. Eng. Sci. 6 (4) (2019).
[27] M. Petrolo, E. Carrera, Best spatial distributions of shell kinematics over 2D meshes for free vibration analyses, Aerotec. Missili Spaz. 99 (2020).
[28] E. Carrera, F. Miglioretti, M. Petrolo, Computations and evaluations of higher-order theories for free vibration analysis of beams, J. Sound Vib. 331 (19) (2012) 4269–4284.
[29] Zaparoli Cunha B., Droz C., Zine A.M., Foulard S., Ichchou M., A review of machine learning methods applied to structural dynamics and vibroacoustic, Mech. Syst. Signal Process. 200 (2023) 110535.
[30] H.-T. Thai, Machine learning for structural engineering: A state-of-the-art review, Structures 38 (2022) 448–491.
[31] R.-T. Wu, R.Jahanshahi. Mohammad, Deep convolutional neural network for structural dynamic response estimation and system identification, J. Eng. Mech. 145 (1) (2019) 04018125.
[32] D. Nath, D.R. Ankit Neog, S.S. Gautam, Application of machine learning and deep learning in finite element analysis: a comprehensive review, Arch. Comput. Methods Eng. (2024) 1–40.

[33] R.E. Meethal, A. Kodakkal, M. Khalil, A. Ghantasala, B. Obst, K. Bletzinger, R. Wüchner, Finite element method-enhanced neural network for forward and inverse problems, Adv. Model. Simul. Eng. Sci. 10 (1) (2023) 6.
[34] H. Bolandi, X. Li, T. Salem, V.N. Boddeti, N. Lajnef, Bridging finite element and deep learning: High-resolution stress distribution prediction in structural components, Front. Struct. Civ. Eng. 16 (11) (2022) 1365–1377.
[35] G. Lee, J.W. Lee, Artificial neural network model to extract modal participation factors for damage localization in beam-like structures, J. Mech. Sci. Technol. (2025) 1–13.
[36] A. Pagani, M. Enea, E. Carrera, Component-wise damage detection by neural networks and refined fes training, J. Sound Vib. 509 (2021) 116255.
[37] S. Lee, H. Kim, Q.X. Lieu, J. Lee, CNN-based image recognition for topology optimization, Knowl.-Based Syst. 198 (2020) 105887.
[38] N. Zobeiry, K.D. Humfeld, A physics-informed machine learning approach for solving heat transfer equation in advanced manufacturing and engineering applications, Eng. Appl. Artif. Intell. 101 (2021) 104232.
[39] V.-T. Tran, T.-K. Nguyen, T.P. Vo, A novel hybrid machine learning and optimization approach for stochastic free vibration analysis of graphene platelets reinforced functionally graded triply periodic minimal surface microplates, Eng. Anal. Bound. Elem. 178 (2025) 106304.
[40] C. Schoenholz, E. Zappino, Petrolo. M, N. Zobeiry, Efficient analysis of composites manufacturing using multi-fidelity simulation and probabilistic machine learning, Compos. Part B: Eng. 280 (2024) 111499.
[41] V. Sze, Y.-H. Chen, T.-J. Yang, J.S. Emer, Efficient processing of deep neural networks: A tutorial and survey, Proc. IEEE 105 (12) (2017) 2295–2329.
[42] K. Pasupa, W. Sunhem, A comparison between shallow and deep architecture classifiers on small dataset, in: 2016 8th International Conference on Information Technology and Electrical Engineering, ICITEE, IEEE, 2016, pp. 1–6.
[43] J. Gu, Z. Wang, J. Kuen, L. Ma, A. Shahroudy, B. Shuai, T. Liu, X. Wang, G. Wang, J. Cai, T. Chen, Recent advances in convolutional neural networks, Pattern Recognit. 77 (2018) 354–377.
[44] K. O'Shea, R. Nash, An introduction to convolutional neural networks, 2015, arXiv e-prints.
[45] L. Alzubaidi, J. Zhang, A.J. Humaidi, A. Al-Dujaili, Y. Duan, O. Al-Shamma, J. Santamaría, M.A. Fadhel, M.A. Al-Amidie, L. Farhan, Review of deep learning: concepts, cnn architectures, challenges, applications, future directions, J. Big Data 8 (2021) 1–74.
[46] M. Petrolo, P. Iannotti, A. Pagani, E. Carrera, Selection of beam, plate, and shell theories using an axiomatic/asymptotic method and neural networks, in: ASME 2024 Aerospace Structures, Structural Dynamics, and Materials Conference:V001T02A012, vol. 04, 2024.
[47] M. Petrolo, P. Iannotti, M. Trombini, A. Pagani, E. Carrera, A machine learning approach to evaluate the influence of higher-order generalized variables on shell free vibrations, J. Sound Vib. 575 (2024) 118255.
[48] Petrolo. M, Iannotti. P., Best kinematics for shell finite elements using convolutional neural networks, Mech. Adv. Mater. Struct. 30 (5) (2023) 1106–1116.
[49] M. Petrolo, E. Carrera, Best theory diagrams for multilayered structures via shell finite elements, Adv. Model. Simul. Eng. Sci. 6 (1) (2019) 4.
[50] M. Cinefra, E. Carrera, A. Lamberti, M. Petrolo, Best theory diagrams for multilayered plates considering multifield analysis, J. Intell. Mater. Syst. Struct. 28 (16) (2017) 2184–2205.
[51] Bathe K.-J., Finite element procedures, 2006.
[52] J.-W. Lin, Artificial neural network related to biological neuron network: A review, Adv. Stud. Med. Sci. 5 (1) (2017) 55–62.
[53] I.H. Sarker, Machine learning: Algorithms, real-world applications and research directions, SN Comput. Sci. 2 (3) (2021) 160.
[54] K. Dong, C. Zhou, Y. Ruan, Y. Li, Mobilenetv2 model for image classification, in: 2020 2nd International Conference on Information Technology and Computer Application, ITCA, IEEE, 2020, pp. 476–480.
[55] Q. Xiang, X. Wang, R. Li, G. Zhang, J. Lai, Q. Hu, Fruit image classification based on mobilenetv2 with transfer learning technique, in: Proceedings of the 3rd International Conference on Computer Science and Application Engineering, 2019, pp. 1–7.
[56] Pastor M., Binda M., Harčarik T., Modal assurance criterion, Procedia Eng. 48 (2012) 543–548, Modelling of Mechanical and Mechatronics Systems.
[57] R.J. Allemang, The modal assurance criterion–twenty years of use and abuse, Sound Vib. 37 (8) (2003) 14–23.